Journal of Visualization, Vol. 1, No. 4 (1999) 379-386

Flow Visualization and PIV Measurement of Flow Field around a Darrieus Rotor in Dynamic Stall

Fujisawa, N.*1 and Takeuchi, M.*2

*1 Department of Mechanical and Production Engineering, Niigata University, 8050 Ikarashi 2, Niigata, 950-2181, Japan.
*2 Department of Mechanical System Engineering, Gunma University, 1-5-1 Tenjin, Kiryu, 376-8515, Japan.

Received 30 July 1998.
Revised 30 October 1998.

***Abstract*:** The flow field around a Darrieus rotor in dynamic stall is studied by flow visualization and PIV measurements. The visualization is carried out by dye injection technique while the phase averaged velocity distributions around the blade are measured by PIV combined with a conditional imaging technique. The results indicate the appearance of dynamic stall phenomenon due to the shedding of two pairs of vortices from the blade during one rotation of the rotor. These stall vortices are produced by the separation of flow over the inner surface of the blade and the formation of roll-up vortices from the outer surface. The second stall vortices develop along the blade and strongly interact with the flow field near the blade, affecting the aerodynamic performance of the rotor.

***Keywords*:** flow measurement, flow visualization, PIV, wind turbine, dynamic stall, fluid machinery.

1. Introduction

The Darrieus rotor is a vertical axis wind turbine operating in a complex unsteady flow environment. During one rotation of the rotor, the blade receives a cyclic force due to the variation of incidence angle of the blade relative to the wind direction. This dynamic variation of the incidence angle produces the dynamic stall of the flow over the rotating blade, which strongly appears at relatively low tip-speed ratios of the rotor during starting and stopping. The appearance of the dynamic stall phenomenon modifies the power performance of the rotor exceeding the steady state prediction (Noll and Ham, 1982). Although this phenomenon acts positively on the power performance of the rotor, the stall vortices generate aeroelastic vibrations on the rotor and on the central column for each operating condition. Therefore, the study of the dynamic stall is very important to design high performance Darrieus rotors (Abramovich et al., 1987).

The dynamic stall of Darrieus rotors has been investigated experimentally in a wind tunnel by measuring the unsteady forces acting on the rotating blade (Laneville and Vittecoq, 1986). The result indicates dynamic variations of lift and drag forces with the presence of a hysteresis loop, which appears at relatively low tip-speed ratios and increases the size of the stall as the tip speed ratio decreases. In order to understand the dynamic stall phenomenon of Darrieus rotors, Brochier et al. (1986) studied the flow fields around a rotor in a water tunnel by measuring the time-averaged flow properties in the wake of a straight-bladed rotor by using laser-doppler velocimetry. The mean velocity distributions of the wake are found to be modified indicating a local maximum velocity, suggesting the presence of stall vortices. The flow visualization study indicates that the flow field consists of a pair of counter rotating vortices, which are formed around the upstream blade and convected downstream through the flow inside the rotor. Recently, PIV measurements have been applied to the whole flow field around the rotor and the variations of the flow field around the rotor have been studied based on the measured velocity field (Fujisawa and Hori, 1997). Although the result shows the flow mechanism of dynamic stall of

Darrieus rotor, the details of the stall vortices are not fully understood because of the poor spatial resolution of the PIV system.

The purpose of this paper is to study the flow mechanism of dynamic stall occurring over the Darrieus rotor blade by using flow visualization and PIV measurement near the blade region. The phase-averaged velocity distribution near the blade is measured with the use of PIV combined with a conditional imaging technique. The flow mechanisms of dynamic stall and the development of the stall vortices downstream are discussed based on these visualizations and measured velocity distributions near the blade.

2. Experimental Apparatus and Procedures

2.1 Modelled Darrieus rotor

Figure 1 shows a cross section of the test Darrieus rotor. The rotor has one straight blade with a section NACA 0018 having a chord length L=10mm and a blade width 135mm, which rotates with a radius, R=30mm. The blade is made of acrylic resin for visualization purposes. It is fixed on an endplate, which is driven by a DC motor with a gear train to rotate at a stable constant speed, and the other end of the blade is kept free. In the present experiment the central column of the Darrieus rotor is removed to observe clearly the flow field inside the rotor.

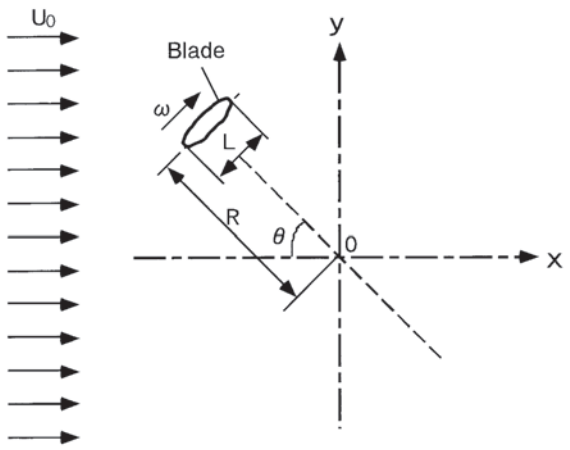

Fig. 1. Darrieus rotor configuration.

2.2 Experimental Apparatus

Figure 2(a) shows the water tunnel used in the present experiment. The working fluid water filled in a tank is powered by a centrifugal pump with a motor of 0.75kW and flows through a bend diffuser as well as a straight diffuser having an outlet cross-sectional area of 500mm × 500mm, a settling chamber, a contraction nozzle, and to a test section of 1600mm length. The uniform velocity U_0 at the test section was set to be U_0=50mm/s and the test rotor was located 450mm downstream of the test section with its axis located horizontally at mid channel height. The cross-sectional area of the test section is 150mm × 150mm. The vertical velocity distribution at the rotor is uniform to an accuracy of ± 3% of the column flow rate. The Reynolds number(=2 RU_0/v) in the present experiment is 3×10^3. Although it is much smaller than that of the prototype rotor, which is Re=10^6~10^7, the flow pattern observed here would agree at least qualitatively, because the flow around the rotor is expected to depend more strongly on the blade geometry and tip-speed ratios than the Reynolds numbers.

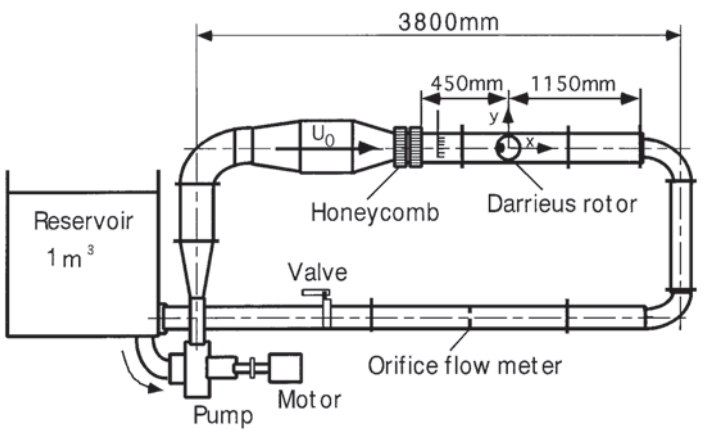

(a)

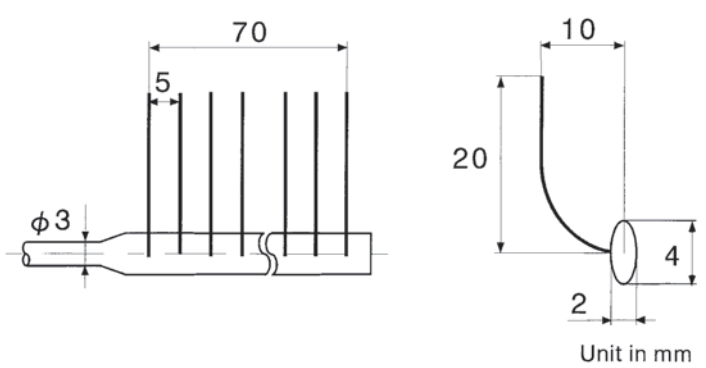

(b)

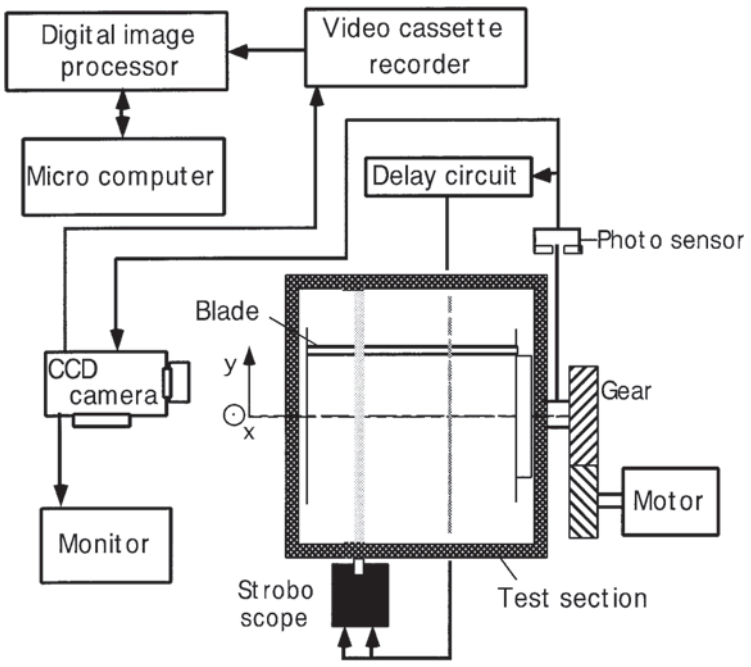

(c)

Fig. 2. Experimental apparatus:
(a) Water tunnel, (b) Dye injection nozzle, (c) PIV measurement system.

2.3 Flow Visualization

The flow around the Darrieus rotor is visualized by the dye injection technique. The injection nozzle, which is shown in Fig. 2(b), is designed to keep the Reynolds number based on the inner diameter of the nozzle (=0.3mm) as small as 15. The injection nozzles are shifted 10mm away from the main pipe to prevent the wake from its development. The Rhodamine B solution is used as the liquid tracer, which is mixed with ethylalcohol to meet with the specific gravity of water. This solution is further diluted by water to a weight concentration of 0.2%. The flow field is visualized by a vertical light sheet of 5mm in thickness from two stroboscopes located over and under the test section, and the observation is made by a CCD camera which has a spatial resolution of 725×492 pixels.

2.4 PIV Measurement

Figure 2(c) shows an experimental arrangement of the present PIV measurement system. The flow field was visualized by a tracer method using plastic microspheres of 30-50 μm diameter with a specific gravity of about 1. The observation of the flow field was made by the same CCD camera as used in the flow visualization experiment. It has a random trigger function, which resets the vertical blanking signal when a trigger signal comes in. In order to capture a set of two images in a short time interval, we used this random trigger function only to reset the vertical blanking signal, and the two sequential images are taken before and after the following vertical blanking signal. For the timing chart of imaging, see Fig. 3. It should be noted that the images captured within the time interval of several fields after the reset motion are found to be unstable owing to the synchronization problem of the camera and VTR (NEC, 1998). The stable images could be recorded on a VTR at 99 msec delay after the reset motion, which is triggered by a signal from a photosensor. When the rotor comes to an expected angular position, the photosensor outputs a trigger signal. The position of the reset motion can be estimated from a simple calculation considering the angular velocity of the rotor and the expected imaging position of the rotor. On the other hand, the imaging of the flow field in a short time interval of 3 msec was realized using two stroboscopes, one controlled by a trigger signal from the photosensor and the other through the delay circuit. Two stroboflashes are obtained from a cylindrical lens located under the test section, which flashes before and after the vertical blanking signal dividing the odd and even field of the frame image. After the visualized images are stored in the VTR, they are digitized by a frame grabber having a spatial resolution of 512×512 pixels with 8 bit in gray level.

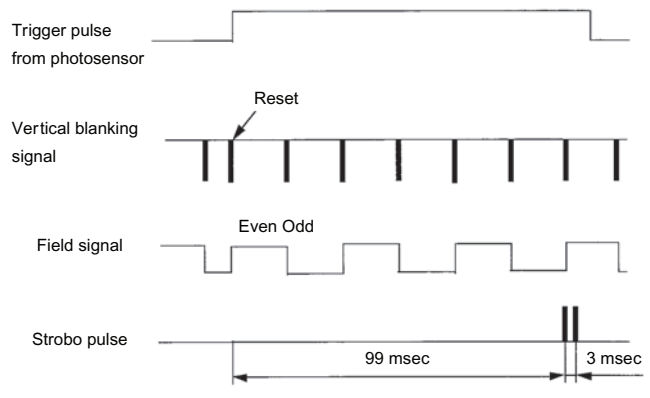

Fig. 3. Timing chart for imaging.

2.5 Image Analysis

The digitized frame images (512×512 pixels) are analyzed by the cross-correlation algorithm (Kimura et al., 1987) for the measurement of velocity vectors. The frame image is separated into two field images (512×256 pixels), each of which is consequently reduced to a image size of 256×256 pixels without distortion of the actual size. Before applying a cross correlation calculation to a set of two images, image enhancement and removal of blade image are carried out in order to minimize the error vectors. The intensity distribution of each image is processed to have the same mean intensity and each distribution is modified in the histogram. These image processings proved to be very effective to obtain a higher correlation coefficient in the analysis, which results in a decrease in error vectors. In the cross-correlation calculations, the matrix size is set to 15×15 pixels and the correlation area

is 25 × 25 pixels, which combination is found to minimize the error vectors in the analysis. In order to obtain a phase averaged velocity distribution, 10 frames of images at the same rotor angles are analyzed and averaged over the velocity vectors at the same position. It should be mentioned that the flow pattern variations in the Darrieus rotor is well correlated with the position of the blade, which allows the phase averaging procedures used in the present experiment.

Figure 4 shows a sample image of the visualized flow field around the Darrieus rotor (a). It consists of two field images visualized by the stroboflashes with an interval of 3 msec. The actual size of the captured image is 25mm × 25mm. The corresponding velocity distributions (b) are obtained from these field images.

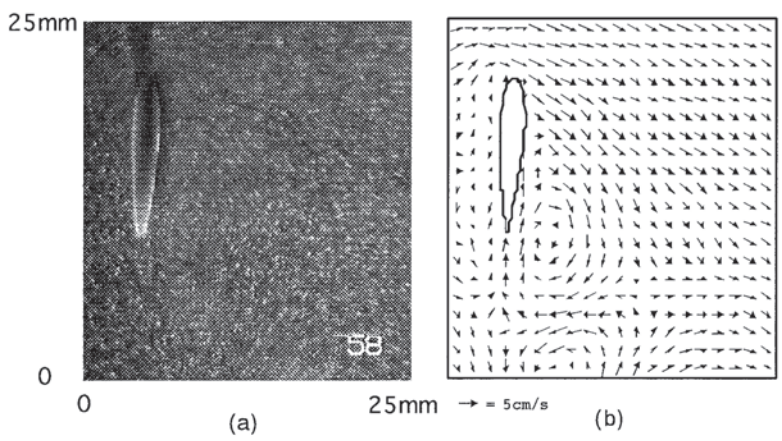

Fig. 4. Sample image and analyzed velocity vectors:
(a) Sample image, (b) Velocity vectors.

3. Results and Discussions

Figures 5(a)~(d) show the flow fields around the Darrieus rotor rotating at a tip speed ratio $\lambda(=R\omega/U_0)=2$ and at five different blade angles $\theta=-45°$, 0°, 45°, 90° and 135°, where ω is the angular velocity of the rotor. Each figure shows the instantaneous flow visualization picture by the dye injection technique, the phase averaged velocity vectors, the vorticity ζ, and the velocity magnitude Vr. Here, the vorticity ζ is defined as $\zeta=(D/U_0)(\partial V/\partial x - \partial U/\partial y)$ and velocity magnitude is $Vr=\sqrt{U^2+V^2}/U_0$, where D is a rotor diameter, and x and y are the streamwise and normal distance, and U and V are corresponding streamwise and normal velocity components, respectively. It is to be noted that the positive sign of ζ indicates the presence of counter clockwise rotating vortices and the negative one, the clockwise rotating ones.

The flow field at the blade angle of $\theta=-45°$ shows the start of the dynamic stall, where the flow over the inner surface of the blade separates around the middle of the blade chord and roll down into the trailing edge of the blade. The flow over the outer surface has the stagnation region near the leading edge of the blade and rolls up into the inner surface of the blade. Therefore, the negative vorticity is distributed over the inner surface with flow acceleration and the positive one in the downstream of the outer surface with flow deceleration. The flow from the inner surface to the outer surface is clearly seen in the velocity vectors and the velocity magnitude over the inner surface of the blade is fairly increased especially around the leading edge, which is due to the moving wall effect of the blade. On the other hand, the separation bubble over the inner surface of the blade develops into an isolated clockwise rotating vortex: it grows in size, as the blade angle increases to $\theta=0°$, which is clearly seen in the visualized picture. However, the presence of the stall vortices was not reported in the visualization study by Brochier et al. (1986). The velocity vectors at $\theta=0°$ show a large recirculating region with clockwise and counter clockwise rotations around the trailing edge of the inner surface, which indicate the presence of second stall vortices. The presence of the stall vortices is also seen in the vorticity map. The map of velocity magnitude shows that the flow accelerates around the leading edge and decelerates over the outer surface, reflecting the moving wall effect of the blade and the stagnation region, respectively. As the blade angle increases to 45°, the first stall vortices over the inner surface of the blade are isolated from the blade, and the second stall vortices appear by the roll-up motion at the trailing edge and the separation over the inner surface of the blade. (The formation of the

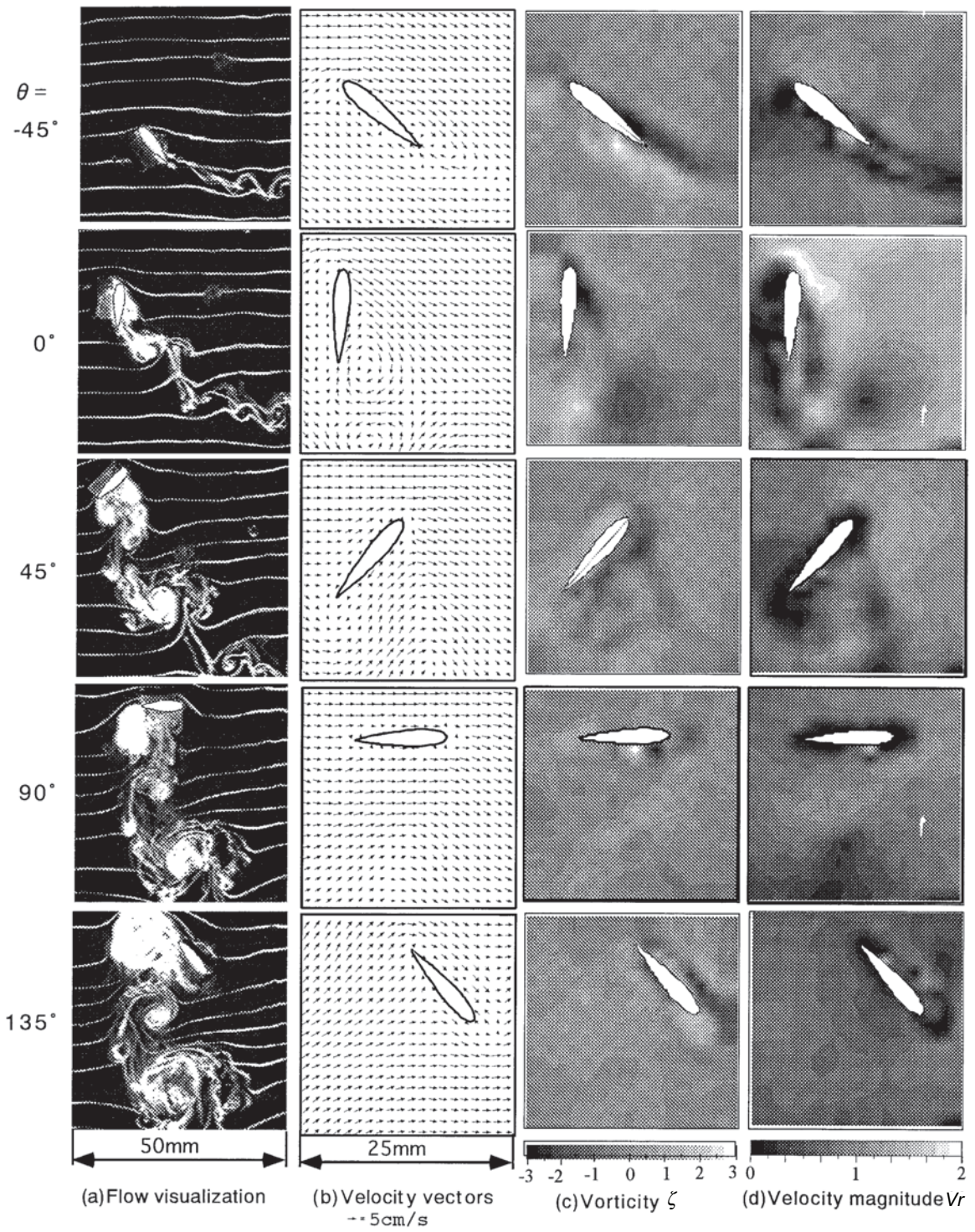

Fig. 5. Flow field around Darrieus rotor at λ=2 (θ=–45°, 0°, 45°, 90°, 135°):
(a) Flow visualization, (b) Velocity vectors, (c) Vorticity ζ, (d) Velocity magnitude *Vr*.

second stall vortices starts around 0 °, which is found from the detail observation in flow visualization study.) The second stall vortices convect downstream along the inner surface of the blade with a velocity smaller than the blade. Therefore, the flow field near the blade is fairly modified by the presence of the second stall vortices, which has also been indicated by the time-averaged velocity measurement by laser-doppler velocimetry and the flow visualization study (Brochier et al., 1986) . The velocity vectors and the vorticity map also show that the flow over the inner surface is strongly modified by the presence of the stall vortices. An increase in the velocity magnitude over the inner surface of the blade shows that the rotor receives an extra torque from the stall vortices, which suggests the power augmentation mechanism in dynamic stall. The visualized flow pattern at θ=45° also indicates the interaction of second pair of vortices with the first pair. As the blade angle increases to 90 °, the second pair of vortices is modified in shape due to the velocity difference between the blade and the stall vortices. As the blade velocity is higher than the convection velocity of the stall vortices, the vortices receive a clockwise circulation by the rotation of the blade. It is expected that the effect of the blade-vortex interaction is still important as the second stall vortices are located near the blade. At the blade angle θ=135°, the second stall vortices are convected toward the wake of the blade and the blade-vortex interaction effect is expected to be weakened. The velocity vectors and the velocity magnitude show that the flow over the inner surface is in stagnation and the flow over the outer surface is strongly curved near the trailing edge of the blade.

Figures 6 and 7 show the flow visualization picture and the measured velocity field around the Darrieus rotor rotating at tip speed ratios λ=1 and 3, respectively. Typical results at the blade angle θ=0°, which indicate the formation of first stall vortices, are shown for comparison. The results show that the second stall vortices are enlarged in size at smaller tip speed ratios and are reduced in size at larger tip speed ratios. It should be mentioned that a part of the second stall vortices rotating in clockwise direction is $2L$ at λ=1, L at λ=2 and $0.7L$ at λ=3, where L is a chord length of the blade. This modification of the flow field is mainly caused by the increase in the incidence angle variations with decreasing tip speed ratios. However, the vorticity distribution and the flow concentration are intensified close to the blade at larger tip speed ratios, which is due to an increase in relative velocities at larger tip speed ratios.

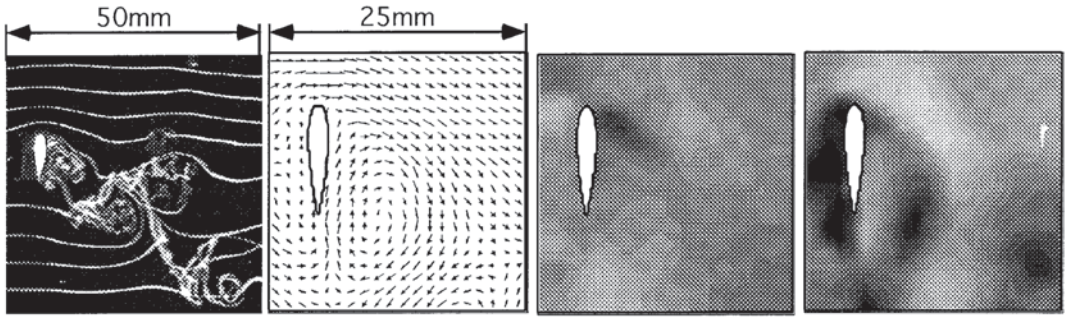

Fig. 6. Flow field around Darrieus rotor rotating at λ=1 (θ=0°):
(a) Flow visualization, (b) Velocity vectors, (c) Vorticity ζ, (d) Velocity magnitude *Vr* (For gray scale see Fig. 5)

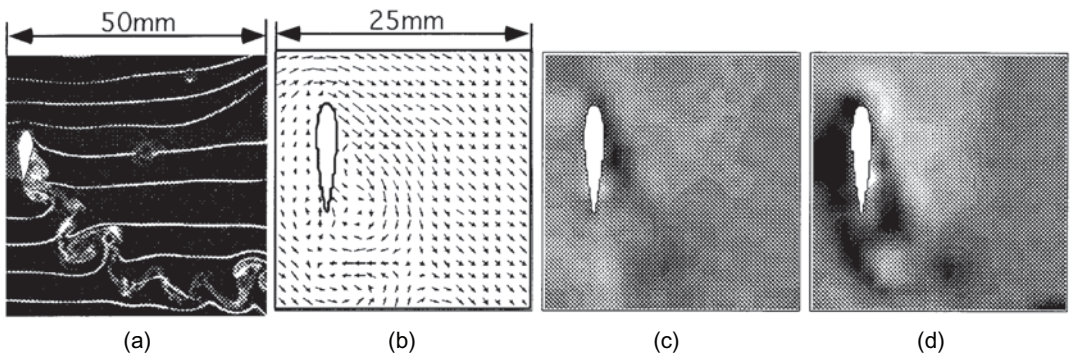

Fig. 7. Flow field around Darrieus rotor rotating at λ=3 (θ=0°):
(a) Flow visualization, (b) Velocity vectors, (c) Vorticity ζ, (d) Velocity magnitude *Vr* (For gray scale see Fig. 5)

4. Conclusions

The flow field around a Darrieus rotor blade in dynamic stall is visualized by dye injection technique and the phase averaged velocity distributions near the blade are measured by PIV combined with conditional imaging technique. The results indicate a variation of the flow pattern in and around the rotor and the formation of stall vortices. It is found that the flow separation over the inner surface of the blade and the corresponding roll up motion of the flow over the outer surface produce two pairs of mushroom type vortices. These stall vortices are formed in one cycle of rotor rotation and the second stall vortices strongly modify the flow field near the downstream side of the blade indicating the presence of a blade-vortex interaction, which may affect the aerodynamic performance of the rotor at low tip-speed ratios.

References

Abramovich, H., Vertical Axis Wind Turbines: A Survey and Bibliography, Wind Engineering, 11-6(1987), 334-343.

Brochier, G., Fraunie, P., Beguier, C., and Paraschivoiu, I., Water Channel Experiments of Dynamic Stall on Darrieus Wind Turbi ne Blades, Journal of Propulsion, 2-5(1986), 445-449.

Fujisawa, N. and Hori, Y., Investigation of Flow Field around a Darrieus Rotor by Flow Visualization and Image Analysis, Trans. JSME, Ser.B, 63-606(1997), 590-595 (in Japanese).

Kimura, I., Takamori, T., and Inoue, T., Image Processing Instrumentation of Flow Velocity Vector Distribution by Using Correla tion Technique; Application to Vortices in the Wake of a Circular Cylinder, Trans. SICE, 23-2(1987), 101-107 (in Japanese).

Laneville, A. and Vittecoq, P., Dynamic Stall; The Case of the Vertical Axis Wind Turbine, ASME Journal of Solar Energy Enginee ring, 108(1986), 140-145.

NEC, Inc., Private communication (1998).

Noll, R.B. and Ham, N.D., Effects of Dynamic Stall on SWECS, ASME Journal of Solar Energy Engineering, 104(1982), 96-101.

Authors' Profiles

Nobuyuki Fujisawa: He received his bachelor of engineering degree in mechanical engineering in 1977 from Iwate University, and master (1979) and doctor (1983) of engineering degrees from Tohoku University in Japan. His doctor thesis is related to the stability and turbulence measurements in curved wall jets . After he joined to Gunma University in 1983, he worked as a research associate in the field of turbomachinery, turbulence modelling and flow visualization. Later he promoted to an associate professor in mechatronics in 1991 and worked in the field of active control and image processing. Since 1997, he has been a professor of Niigata University and continuing the research in active control of flow and flow-induced noise, flow visualization and image processing and PIV in thermal and fluid phenomena.

Mitsuyoshi Takeuchi: He received his bachelor (1996) and master (1998) of engineering degrees in mechanical engineering from Gunma University in Japan. He is currently an engineer working in Nihon Kohden Corporation in Japan.